Vol. 25, No. 2(2026) Sim26649

Revista Mexicana de Ingeniería Química

Numerical modeling of synovial fluid behavior considering Newtonian and non-Newtonian approaches

Modelización numérica del comportamiento del líquido sinovial considerando enfoques Newtonianos y no Newtonianos

N. Martínez-Gutiérrez[1,2], L.A. Ibarra-Bracamontes[1*], L.F. Fuentes-Cortés[3,4], S.R. Galván-González[1]

[1] *Facultad de Ingeniería Mecánica, Universidad Michoacana de San Nicolás de Hidalgo, Francisco J. Múgica S/N, 58030, Morelia, Michoacán, México.*

[2] *Tecnológico Nacional de México, Instituto Tecnológico de Morelia, Departamento de Ingeniería Metal-Mecánica, Morelia, Michoacán, 58120, México.*

[3] *IMT Atlantique, Department of Energy Systems and Environmental GEPEA, 4 rue Alfred Kastler, F-44307, Nantes, Francia.*

[4] *Maestría en Ingeniería para la Sostenibilidad Energética, Universidad Intercultural Indígena de Michoacán, Carretera Pátzcuaro-Huecorio Km 3, Pátzcuaro C.P. 61614, México.*

Received: August 15, 2025; Accepted: March 21, 2026

Abstract

This work compares two approaches, Newtonian and non-Newtonian, for numerical modeling of synovial fluid behavior under deformation conditions. Fluid viscosity and velocity are analyzed, along with the total pressure in the system during deformation. The Power Law and Carreau approaches are used for addressing the non-Newtonian behavior of the fluid. The results indicate that lower porosity in the articular cartilage region leads to higher fluid velocity in that region, and in the non-Newtonian case, this results in a reduction in synovial fluid viscosity. The Carreau model, which includes a relaxation parameter, allows for smoother transitions in viscosity during deformation. It was found that increasing the deformation distance or decreasing the permeability in the porous medium raises the total pressure. The proposed model enables control of physical variables that could represent the behavior of a biological system under normal conditions or with some deficiency.

Keywords: synovial fluid; articular cartilage; non-Newtonian fluid; Power Law model; Carreau model; simulation.

Resumen

Este trabajo compara dos enfoques, newtoniano y no newtoniano, para la modelización numérica del comportamiento del fluido sinovial en condiciones bajo deformación. Se analiza la viscosidad y la velocidad del fluido, así como la presión total en el sistema durante la deformación. Los modelos no newtonianos utilizados fueron: Ley de Potencia y Carreau. Los resultados muestran que cuanto menor es la porosidad en la región del cartílago articular, mayor es la velocidad del fluido en dicha región y en el caso no Newtoniano, esto provoca una reducción de la viscosidad del fluido sinovial. El modelo de Carreau al incluir un parámetro de relajación permitió obtener transiciones más suaves en la viscosidad durante la deformación. Se obtuvo que al aumentar la distancia de deformación o al reducir la permeabilidad en la región porosa, la presión total aumenta. El modelo propuesto permite controlar variables físicas que permiten representar el comportamiento de un sistema biológico en condiciones normales o con alguna deficiencia.

Palabras clave: líquido sinovial, cartílago articular, fluido no Newtoniano, modelo Ley de Potencia, modelo de Carreau.

* *Corresponding author. E-mail*: laura.ibarra@umich.mx ;

https://doi.org/10.24275/rmiq/Sim26649

ISSN:1665-2738, *issn-e*: 2395-8472

1 Introduction

From an engineering point of view, dealing with biological fluids, especially those associated with the human body, represents a great challenge due to the variations in properties associated with degradation processes and heterogeneity in compositions of biological fluids (Kumavat *et al*., 2021; Zambrano *et al*., 2018). Despite the above, the development of synthetic fluids, prostheses, and composites has made it possible to improve the quality of life of people affected by chronic degenerative diseases (Abraham and Venkatesan, 2023). In the case of synovial fluid, one of the challenges is the evaluation of viscosity under deformation conditions, which are common in patients suffering from osteoarthritis and conditions related to rheumatism (Oliviero and Mandell, 2023).

Osteoarthritis is the most common form of arthritis, affecting approximately 7.6% of the worldwide population (Perrucio *et al*., 2024). This disease mainly affects the articular hyaline cartilage in the load-bearing joints such as the knee, hip, and shoulder (Märtens *et al*., 2022). Due to its prevalence and diversity in terms of progression in different patients, the analysis of synovial fluid has been the subject of multiple approaches, including invasive (Sajan *et al*., 2022) and non-invasive techniques (Oei *et al*., 2022), as well as modeling strategies (Pearce *et al*., 2020).

The main functions of synovial fluid are, first, it participates in the nutrition of articular cartilage as a carrier in the transport of nutrients. Second, it supports the mechanical function of the joint by lubricating the joint surfaces (Brannan and Jerrard, 2006). In both cases, it is necessary to know the distribution of flow throughout the synovial cavity. (Sadique *et al*., 2023) Addressed studies on fluid-structure interactions, focusing on those associated with cartilage. In that study, a proportional relationship between the permeability of the articular cartilage and the speed of displacement of the synovial fluid within the cartilage is identified. This means that as cartilage permeability increases, the rate of synovial fluid displacement also increases. In other words, more permeable cartilage allows for greater synovial fluid flow, which is crucial for cartilage lubrication.

To capture variations associated with health conditions and conduct contrast studies, research has been performed based on modeling strategies in both patients with healthy knees (Hasnain *et al*., 2023) and those with varying degrees of osteoarthritis development (Chhimwal *et al*., 2023). Another factor that must be considered when modeling a synovial joint is the variability in cartilage size, whether in healthy individuals or those affected by osteoarthritis. The reported thickness of knee cartilage ranges from 1.15 to 2.60 mm in non-arthritic patients (Giurazza *et al*., 2024). Synovial fluid volume in an average knee varies between 0.5 and 4.0 ml. This range depends on health conditions or age (Kraus *et al*., 2007). Cartilage is known to be a viscoelastic, porous, and permeable tissue, containing 20% solid by dry weight and 80% fluid phase under healthy conditions (Eschweiler *et al*., 2021).

Another important factor to consider is the geometry of articular cartilage, as it plays a key role in the phenomenon under analysis. In the work of Pekkan *et al*. in 2003 (Pekkan *et al*., 2003) a geometry with a curved surface has been proposed because it is thought to reduce shear stress peaks and improve synovial fluid circulation compared to flat surfaces. This supports the proposals of authors who have used this type of geometry, whether in mathematical or numerical. The axisymmetric squeeze-film approach, as reported by P. Jurczak (2006) and other authors (Jurczak *et al*., 2006; Ruggiero & D'Amato, 2010; Walicka & Walicki, 2004; Walicki & Walicka, 2000), provides a valuable framework for studying hydrodynamic pressure behavior and the influence of non-Newtonian rheology under simplified geometric conditions.

The use of simplified models has allowed the capture of variations in permeability, porosity, and the relationship between viscosity and shear rate, among other properties, offering a more accessible computational framework. In addition to the axisymmetric squeeze-film configuration, other geometric idealizations have been used in the literature to study joint behavior. Among the most commonly used are the Ball-on-Plane, Ball-in-Socket, Elliptical Ball-in-Socket, and Spherical Ball-in-Socket configurations. Other parameters incorporated to model a synovial cavity include cartilage deformation (Halonen *et al*., 2014) or the percentage deformation of the fluid zone due to joint loading (Martínez-Gutiérrez *et al*., 2016).

In contrast to a three-dimensional model, this two-dimensional axisymmetric model represents an idealized geometry where the pressure field depends exclusively on the radial coordinate. This two-dimensional axisymmetric model does not take into account the common geometric irregularities observed in a real knee joint, such as variations in cartilage thickness, irregular morphologies of the synovial cavity, and the actual tibiofemoral geometry of the knee.

Modeling fluid-structure interactions in cartilage and synovial fluid is highly complex due to the diverse biophysical factors. It increases the likelihood of facing alterations associated with health disorders or diseases (Liao *et al*., 2020). Therefore, modeling strategies vary depending on the approach, data availability, or computational capacity. Consequently, different authors have used representative models for synovial fluid as a Newtonian fluid (Chhimwal *et al*., 2023) or as a non-Newtonian fluid (Ouerfelli *et al*., 2024).

From a purely modeling perspective, the Newtonian approach, although idealized, offers computational advantages, such as eliminating variables associated with viscous and pressure effects. Even so, the information it provides can be exploited to characterize the fluid's behavior under standard conditions. However, non-Newtonian models, despite their complexity in terms of solution and computational cost, can provide a more realistic representation of the system (Simou *et al*., 2022; Hasnain *et al*., 2023). Despite the efforts outlined above, it is important to compare the two approaches to move towards a general and comprehensive modeling strategy. Considering the current context of developing computational tools based on the application of black box and data-driven models, it is essential to have reference models based on fundamental physical principles to compare performance (Botu *et al*., 2017; Fuentes-Cortés *et al*., 2022).

In this work, a comparison between the performance of a Newtonian model and two non-Newtonian models for synovial fluid is presented. These non-Newtonian approaches are based on the Power Law and Carreau. The Carreau model has been reported to be helpful in representing fluids whose viscosity gradually changes with shear rate and can be approximated to both pseudoplastic and near-Newtonian behavior at low shear rates (Kren *et al*., 2007; Brujan, 2011; Madkhali *et al*., 2016). On the other hand, in the case of non-Newtonian fluids, the Power Law model is one of the most widely used models currently for the study of synovial fluid (Hasnain *et al*., 2023; Ouerfelli *et al*., 2024). Therefore, this work contributes to the discussion regarding numerical modeling of synovial fluid behavior in a synovial cavity, considering the following aspects:

The biological system model was scaled with values corresponding to those of a synovial cavity found in the literature. The main properties analyzed were the viscosity of the biofluid, the velocity of the moving wall, and the properties of the porous medium, such as permeability and porosity. A comparison is made between the Newtonian, Carreau, and Power Law models, which are commonly used independently in literature. The analysis considers, for comparison purposes, equal boundary conditions for each of the modeling strategies presented in such a way that the convenience of each modeling strategy is elucidated.

In the present work, both Newtonian and non-Newtonian fluids are analyzed. Although the primary focus is on biological media, the scope of their applications extends beyond this field, as they are also widely used in industry. When used as lubricants, these fluids play a crucial role in reducing friction and wear in mechanical systems, thereby enhancing operational efficiency and extending component service life. The findings of this study may serve as a foundation for optimizing the design of elements operating under severe conditions, such as industrial bearings subjected to high loads and low speeds. The incorporation of non-Newtonian fluid models has been shown to increase load-carrying capacity, as emphasized by Holmberg and Erdemir in their analysis of bearing systems (Holmberg & Erdemir, 2017). These components are essential in diverse applications, including turbomachinery, aeronautical engines, mechanical equipment, and automation, where reliability and efficiency are crucial. Bearings must also withstand extreme environments characterized by high loads and temperatures, ensuring the stability and performance of industrial systems (Siddiqui *et al*., 2025).

The objective of this paper is to compare classical models for analyzing the behavior of synovial fluid when flows are induced by the application of loads that deform the fluid region. The Power Law and Carreau models have been chosen to highlight the key differences between the Newtonian and non-Newtonian approaches.

2 Methodology

The numerical model is based on the geometry commonly used in the literature (Jurczak, 2006; Walicki and Walicka, 2002; Martínez-Gutiérrez *et al*., 2016), where a bio-bearing is proposed, which is composed of two regions: the fluid region for the synovial fluid (SF) and the porous medium region to model an articular cartilage (AC). The two regions, AC and SF, represent the synovial joint of the knee, specifically the synovial cavity. This cavity is mainly composed of the femur and tibia bones, articular cartilage, and synovial fluid. By generating a vertical movement in the femur bone, synovial fluid is moved, which allows, on the one hand, the fluid to enter the articular cartilage. This movement occurs during cartilage nourishment. On the other hand, it is the displacement in the same area of the synovial fluid that contributes to the cushioning of the knee. The movement described above is the one that occurs in a usual human displacement. Therefore, the first step is to apply an initial velocity in the model, which allows simulating the movement of the femur.

Fig. 1 (a) shows the geometry of the model where a velocity (V) is applied in a downward vertical direction, which generates a displacement (e) and a deformation in the upper region, or SF, causing the fluid to move both in the SF region and in the lower

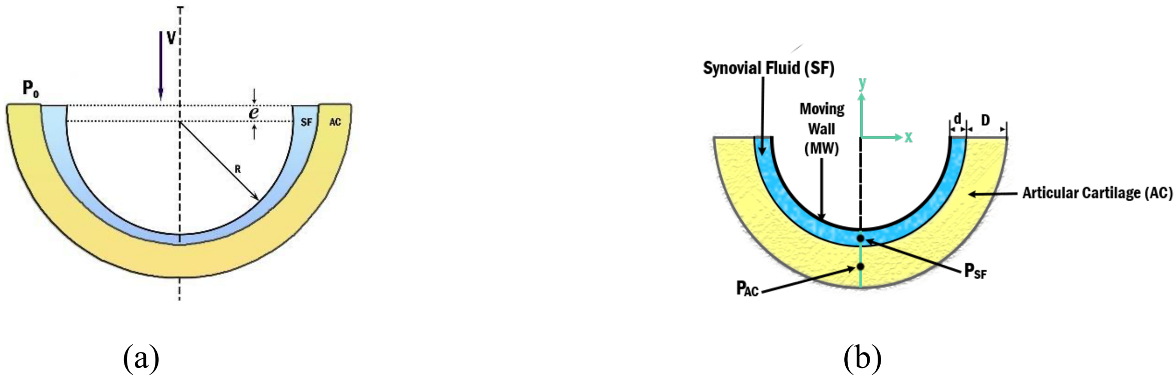

Figure 1. Geometry of the numerical model: (a) Bio-bearing, (b) numerical meshing.

region, or AC. Figure 1(b) shows the curve called the moving wall, which moves with a velocity V, and two selected points to monitor the fluid. These points are in the central position along the vertical axis, both in the SF region, identified as P_{SF} and the other in the AC region, identified as P_{AC}. At each of these points, the values taken by variables such as pressure, velocity, and viscosity were recorded over time.

2.1 *Governing equations and numerical model*

This section describes the modeling and computational aspects associated with the problem addressed. First, the expressions governing the physics of the fluid-cartilage system are presented, followed by linear and nonlinear computational approaches.

2.1.1 *Hydrodynamic considerations*

As shown in Fig. 1, the proposed model comprises two regions: SF and AC. To describe flow velocities, the continuity equation, based on the conservation of mass, is used. It leads to considering the principle that the mass in a control volume remains constant. For simplicity, it is assumed that the system can be studied as a two-dimensional domain as a first approximation. Therefore, if a two-dimensional system and an incompressible fluid are considered, the continuity equation is as follows:

$$\nabla \cdot \mathbf{u} = 0 \tag{1}$$

where $\nabla \cdot \mathbf{u}$ is the divergence of the velocity field, which must vanish for an incompressible fluid.

2.2 *Momentum equations*

The equation of momentum is one of the fundamental equations of fluid mechanics. It is derived directly from the second law of Newton applied to a control volume within the fluid and describes how the velocity of a fluid changes in time and space due to the action of forces. These forces can be surface forces (such as pressure and viscosity) or body forces (such as gravity). For a Newtonian fluid, by having a control volume in two dimensions. The momentum equation for the system can be expressed as follows:

$$\rho\left(\frac{\partial \mathbf{u}}{\partial t} + \mathbf{u} \cdot \nabla \mathbf{u}\right) = -\nabla p + \mu \nabla^2 \mathbf{u} + \rho \mathbf{f} \tag{2}$$

where ρ is the fluid density, $\frac{\partial \mathbf{u}}{\partial t}$ is the local (temporal) acceleration, $\mathbf{u} \cdot \nabla \mathbf{u}$ represents the viscous diffusion of momentum, p is the pressure, $\mu \nabla^2 \mathbf{u}$ represents the viscous diffusion of momentum, u is the velocity vector, and $\mathbf{f}$ are the external forces.

Equation (3) establishes the basis for the subsequent numerical formulation, where non-Newtonian constitutive models are incorporated to describe the rheological behavior of synovial fluid.

As outlined in the introduction, synovial fluid exhibits non-linear behavior between viscosity and shear rate; therefore, for non-Newtonian models, as the viscosity is not constant, the momentum equation is modified as follows:

$$\rho\left(\frac{\partial \mathbf{u}}{\partial t} + \mathbf{u} \cdot \nabla \mathbf{u}\right) = -\nabla p + \nabla \cdot \boldsymbol{\tau} + \rho \mathbf{f} \tag{3}$$

where $\boldsymbol{\tau}$ is the viscous stress tensor.

The Power Law model is widely used to describe the rheological behavior of non-Newtonian fluids. This model has been applied to characterize the behavior of synovial fluid due to its ease of implementation in simulations (Hasnain *et al.*, 2023). Therefore, it could model nonlinear behavior in shear rate ranges for physiological values. The apparent viscosity (η_{app}) of a non-Newtonian fluid depends on the shear rate. For the Power Law model, apparent viscosity is expressed as follows:

$$\eta_{app} = \kappa (\dot{\gamma})^{n-1} \tag{4}$$

where κ is the consistency index, n is the Power Law index and $\dot{\gamma}$ is the magnitude of the shear rate.

One advantage of using the Carreau model is to capture a gradual transition in viscosity between low and high shear rates. For the Carreau model, η_{app} is expressed as:

$$\eta_{app} = \eta_\infty + (\eta_0 - \eta_\infty)\left[1 + (\lambda\dot{\gamma})^2\right]^{\frac{n-1}{2}} \tag{5}$$

where η_∞ is the viscosity at the limit of high shear rates, η_0 is the viscosity at rest (or viscosity at the limit of low shear rates), λ is a characteristic time parameter that determines the transition range between low and high shear rate behaviors, and n is the Power Law index, which indicates the nature of the fluid. In this case $n < 1$, it represents a pseudoplastic fluid.

To introduce permeability, an additional term was included to account parameters for viscous resistance and inertial resistance, as shown in the following equation:

$$\rho\left(\frac{\partial \mathbf{u}}{\partial t} + \mathbf{u}\cdot\nabla\mathbf{u}\right) = -\nabla p + \nabla\cdot\boldsymbol{\tau} - \frac{\mu}{\beta}\mathbf{u} + \rho\mathbf{f} \tag{6}$$

where β is the permeability of the porous medium.

In the AC zone, the model uses the Superficial Velocity Porous Formulation to account for the porosity of the medium (Bear Jacob, 1972; Ingham Derek B, 2003). The porous medium is modeled as a continuum using the concept of Representative Elementary Volume (REV), which ensures that macroscopic properties are independent of the size of the analyzed volume. Based on this idea, volumetric averages allow for the consistent definition of Darcy velocity and the average fluid velocity. This formulation provides a relationship between the microscopic behavior of flow in the pores and its effective representation on a continuous scale. This is expressed in equation 7 (Nield *et al*., 2013):

$$\mathbf{u} = \frac{\mathbf{u}_D}{k} \tag{7}$$

where $\mathbf{u}_D$= Darcy velocity, $\mathbf{u}$ = Intrinsic average velocity, and k = Porosity.

Since the physical phenomenon exhibits variation in porosity within the cartilage, the current model proposes two fixed porosity values, k = 0.2 and k = 0.8, for low and high porosity respectively, in the articular cartilage zone (AC).

2.3 *Boundary conditions and physical properties*

The dimensions of the system were obtained from an anthropometric study (Ziylan *et al*., 2002) and adapted to the numerical model conditions (Martínez-Gutiérrez *et al*., 2016). An interface was defined between the articular cartilage (AC) and synovial fluid (SF) regions to establish a boundary condition. Through this interface, the synovial fluid flows into the articular cartilage zone.

Initially, a comparison was made between the proposed models and experimental data from a synovial joint study by Smith, who examined the apparent viscosity of synovial fluid (LS) as a function of shear rate (Smith *et al*., 2014). These data were used to determine the parameters for the non-Newtonian fluid models, specifically the Power Law and Carreau models, as shown in Fig. 2.

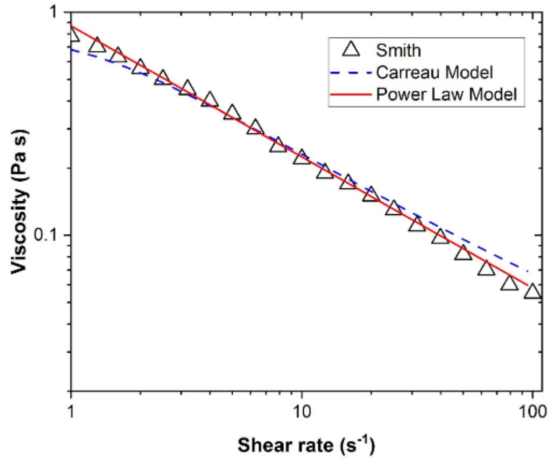

Figure 2. Smith's experimental data and the adjustments made to derive the parameters for both the Power Law and Carreau models.

- To model the viscosity of SF, two values were considered for the Newtonian case: 0.001003 Pa·s for water (considered as an initial reference value) and 0.6 Pa·s for synovial fluid (Moghadam *et al*., 2015). Two non-Newtonian models were also adapted based on the experimental data reported by Smith *et al*. (2014).

- For the Non-Newtonian Power Law model: κ = 0.8695 (kg·s)1/m, n = 0.412.

- For the Carreau model: λ = 0.8679 s, n = 0.412, η_0= 0.8 Pa·s, and η_∞ = 0.01 Pa·s.

- The speeds (V) of the moving wall considered in this study are 35, 40, 45, and 50 mm/s.

- For the AC region, two porosity values were used: k = 0.2 and 0.8; three permeability values: $\beta = 10^{-14}$, 10^{-10}, 2.6×10^{-8}, and 10^{-7} m^{-2}. The synovial cavity was modeled as an open system, with a pressure boundary condition of P_0 = 0 Pa at the ends.

- The curvature radius of the moving wall, R = 38.62 mm (Ziylan T & Murshed K.A, 2002); the thickness of the initial semicircular-shaped fluid zone, d= 0.1062 mm; the cartilage thickness, D=6.0 mm; and the density of the synovial fluid was considered to be 1000 $\frac{Kg}{m^3}$ (Moghadam *et al*., 2015).

- Two values for the dimensionless displacement of the moving wall, $\varepsilon = e/d$, were proposed: 0.1 and 0.5; ε represents the ratio of displacement of the moving wall regarding the thickness of the fluid region: 0.1 indicates a 10% displacement of the thickness of the synovial fluid region (SF), and 0.5 indicates a 50% displacement of the thickness of the synovial fluid region.

2.4 Computational model

To solve the numerical model based on the geometry in Fig. 1, a triangular mesh with 132593 nodes was used, and mesh refinement was performed in the SF zone. To validate the mesh, Richardson extrapolation (Phillips & Roy, 2014) was applied. For this purpose, three meshes with different densities were proposed: mesh 1 (66,276 nodes), mesh 2 (132,593 nodes), and mesh 3 (264,547 nodes). The three meshes were systematically refined with a refinement ratio of 2. Initially, the average recovery pressure was calculated at the interface as a reference zone between the synovial fluid and the articular cartilage for evaluating the numerical model. The values obtained for the recovery pressure for each mesh were: mesh 1 (156.56863 Pa), mesh 2 (157.38852 Pa), and mesh 3 (159.75201 Pa). The Richardson extrapolation obtained during the analysis was 157.132 Pa, which is close to 157.38852 Pa; therefore, the number of nodes selected for the model was that of mesh 2. A safety factor of 1.25, a mesh convergence index of $GCI_{12} = 0.347\%$ (mesh refinement ratio) and $GCI_{23} = 0.996\%$, and a convergence range of 1.5. These results confirm that the selected mesh guarantees numerical independence, with an uncertainty of less than 2%.

Remeshing and smoothing techniques were implemented during the movement of a moving wall in the SF region (see Fig. 1b). The displacement of the moving wall was generated using a connecting rod-crank mechanism for the movement of a piston (Norton, 2009). The displacement of the moving wall was based on equation 8 expressed as follows:

$$y = r - r\cos\theta + \frac{r^2}{2l}\sin^2\theta \tag{8}$$

where: r = crank radius, l = connecting rod length, θ = crank angle, y = piston position, in our case is the moving wall position. The assessment was carried out for a θ range from 0 to 90°, to indicate that the displacement made is only a quarter of the cycle.

A user-defined function (UDF) was programmed to indicate the conditions of the displacement. The proposed model was executed in Ansys Fluent, which uses the finite-volume method to discretize the partial differential equations that govern fluid flow (Ansys®). For the finite-volume method, the domain is first divided into control volumes (mesh generation). Then the equations are integrated over the control volume, applying Gauss's divergence theorem, which is a vector equation for the time, convective, diffusive, and source terms, generalized to any conservative transport property. See Eq 9.

$$\frac{\partial(\rho\lambda)}{\partial t} + \nabla\cdot(\rho\mathbf{u}\lambda) = \nabla\cdot(\Gamma\nabla\lambda) + s_i \tag{9}$$

where the first term is the temporal term, the second is the convective term, the third is the diffusive term, and the last is the source term. (Yeoh & Yuen, 2009)

Finally, the discretized general equation is applied at the centroid of each cell. The simulation was carried out using a Semi Implicit Method for Pressure Linked Equations (SIMPLE), a first-order method. SIMPLE estimates a pressure field and then solves the momentum equation using that pressure to obtain approximate velocity fields. Next, it calculates the mass flow rates and solves the equation to obtain corrected pressure. Subsequently, it calculates the corrected velocity, resulting in corrected velocity fields that satisfy the continuity equation. Finally, it solves the continuity equation using the corrected velocity field. If the solution has not converged, it will recalculate the momentum equation using the new pressure, making it an iterative process.

The proposed numerical model was validated for Newtonian fluid conditions by comparison with the analytical solution proposed by Jurczak (2006). Jurczak's work employed a dimensionless pressure expressed in equation (10) as follows:

$$\widetilde{p} = \frac{(p-p_0)d^2}{\mu R^2\dot{\varepsilon}} \tag{10}$$

where $p = p(\varphi)$ is the angular pressure, p_0 is the pressure at $\varphi = \pm 90$ (the angular ends of the fluid zone), μ is the fluid viscosity, and R is the curvature radius of the moving wall, $\dot{\varepsilon}$ is the deformation rate of the fluid zone; d is the thickness of the initial semicircular-shaped fluid zone (see Figures 1a and 1b).

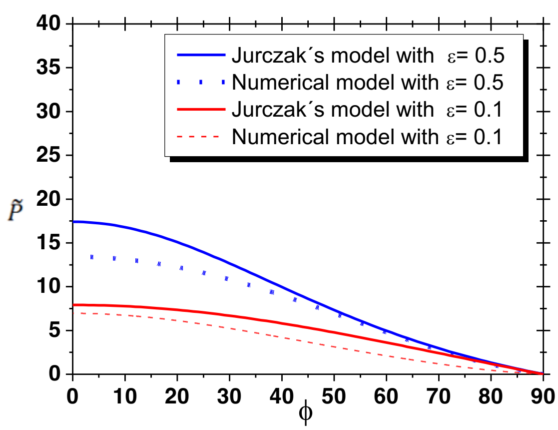

Figure 3. Dimensionless angular pressure obtained with the numerical model and the analytical model by Jurczak (2006), with $\varepsilon = 0.1$, and 0.5, $\kappa = 0.2$.

Fig. 3 shows the behavior of the model of Jurczak, compared to the model proposed in the present study, for Newtonian behavior. The similarity in the pressure profiles indicates that the governing equations, boundary conditions, and numerical discretization capture properly the hydrodynamic behavior predicted by the analytical model. This validation ensures that the computational framework can be extended with confidence to non-Newtonian conditions, where analytical solutions are limited. A more detailed explanation of the validation of the numerical model can be found in a previously published work (Martínez-Gutiérrez *et al*., 2016).

In addition, the Reynolds number was calculated for three initially proposed viscosity values, using water as the reference. The Reynolds number was calculated as shown in equation 11:

$$Re = \frac{\rho V d}{\mu} \tag{11}$$

where ρ is the density of synovial fluid, μ is the dynamic viscosity, d is the characteristic length of the system, which corresponds to the initial thickness of the fluid zone, and V is the velocity of the moving wall. According to the system's geometry, the initial thickness value considered was d= 0.1062 mm, which remains constant (Martínez-Gutiérrez *et al.*, 2016). Furthermore, for the viscosity values used, 0.001003 $\frac{Kg}{m \cdot s}$, 0.6 $\frac{Kg}{m \cdot s}$, and 0.8 $\frac{Kg}{m \cdot s}$, the range of Reynolds numbers obtained were from 4.6E-03 to 5.29. In this model, heat transfer within the system was not considered; only changes in viscosity as a function of shear rate were taken into account. According to the values obtained for the Reynolds number and the flow lines of the velocity fields, the results are within a laminar flow regime.

3 Results

This section shows and discusses the results of the numerical model and addresses the relevant aspects that differentiate the Newtonian and non-Newtonian approaches. In the first part, the comparison between Newtonian and non-Newtonian models is addressed. Subsequently, the details of the non-Newtonian models are discussed.

For comparison between Newtonian and non-Newtonian approaches, emphasis is placed on the behavior of apparent viscosity. Fig. 4 shows the behavior of the Newtonian cases for both regions, SF and AC in which the viscosity remains constant, with values of 0.001003 Pa·s and 0.6 Pa·s. The non-Newtonian models, Carreau and Power Law, present a fast decrease in viscosity in a short period of time in the SF zone. The abrupt reduction in viscosity is a consequence of the dependence of viscosity on the shear rate.

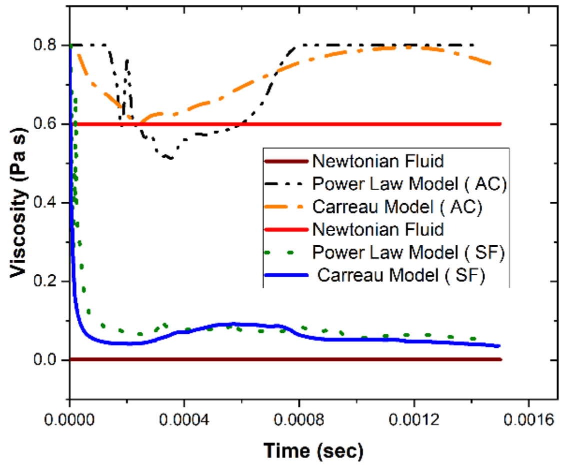

Figure 4. Viscosity vs time in SF and AC regions using: Power Law model, Carreau model, two Newtonian fluids (high and low viscosity), V=50 mm/s, e=0.5, κ=0.8, β=2.6E-8.

Non-Newtonian models represent a pseudoplastic fluid. In the case of the Power Law model, as the shear rate ($\dot{\gamma}$) increases, the shear stress increases at a lower rate (see Eq. 4), which means that the apparent viscosity of the fluid decreases rapidly. Considering the Power Law index, for low values of n, the fluid becomes less viscous as the shear stress increases (see Eq. 5). In the case of the Carreau model, when the shear rate is low, the viscosity is close to η_0, for this model, its value corresponds to 0.8 Pa·s. It is consistent with the behavior observed in Fig. 4. When the shear rate increases, the viscosity decreases sharply until it reaches values close to water viscosity. On the other hand, in the case of the AC region, it can be observed that the model of Carreau registers viscosity variations smoothly compared with the model of Power Law. Due to its mathematical formulation, the Carreau model includes a characteristic time parameter, which allows for describing the transition between viscosity at low and high shear rates. The Carreau model is designed to represent a gradual transition, not an abrupt one.

Fig. 5 shows the results of the total pressure behavior for three models: two Newtonian and one non-Newtonian. As the moving wall moves, the fluid region undergoes greater thinning in the direction of displacement, as shown in Fig. 1(a). This thinning corresponds to the maximum value of total pressure in the system. For the Newtonian case with the highest viscosity (0.6 Pa·s), the highest total pressure is obtained, reaching values up to 100 MPa. In this case, the fluid shows greater resistance to moving in its environment. In the case of the Carreau model, as it is a function of the shear rate, the apparent viscosity varies, and its maximum pressure is close to 10 MPa.

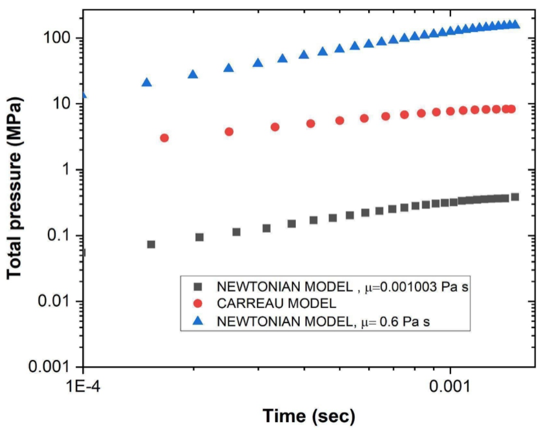

Figure 5. Total pressure vs time for two Newtonian fluids and one non-Newtonian fluid in the SF region, V=50 mm/s, ε=0.5, k = 0.8, β=2.6E-8.

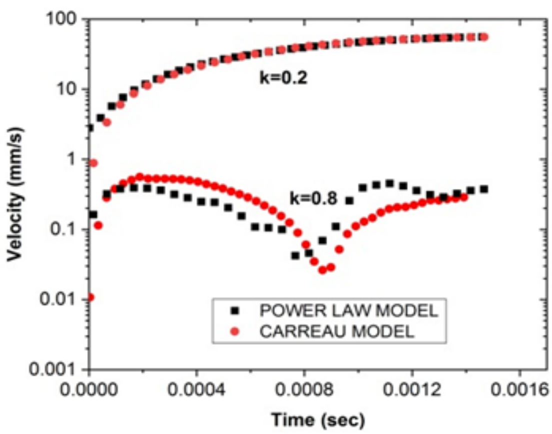

Figure 6. Speed vs time comparing the two non-Newtonian models for different porosity values in the SF region, V=50 mm/s, ε=0.5, β=2.6E-8.

In the Newtonian case with low viscosity (0.001003 Pa·s), the lowest total pressure value is obtained because it generates low resistance to flow, reaching values less than 1 MPa.

Fig. 6 shows the velocity results as a function of time when the porosity in the AC zone is varied. The velocity results were measured at the point P_{SF} located in the central part of the SF region, as shown in Figure 1(b). The results show that, at a low porosity (k=0.2), the velocity has a more uniform behavior for both non-Newtonian models. Velocities in the SF region reached values of approximately 60 mm/s. On the other hand, in the case of high porosity (k=0.8), the velocities fluctuated around 0.1 mm/s in both models. Therefore, no significant differences in velocity were observed when comparing both non-Newtonian models when porosity was varied.

The fluid velocity in the two regions under study is shown in Fig. 7. As mentioned above, fluid velocities were measured at two reference points: P_{SF} is located at the centroid of the SF region, and P_{AC} is located at the centroid of the AC region (see Fig. 1(b)).

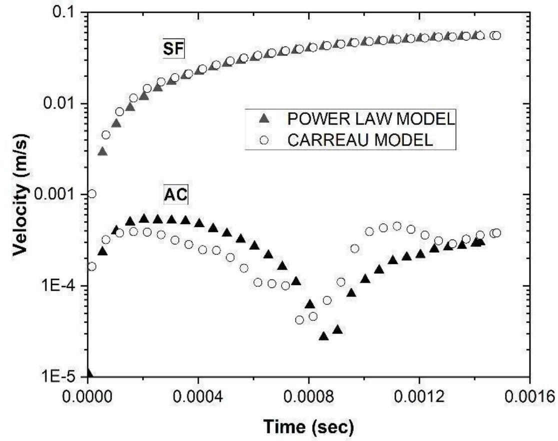

Figure 7. Velocities vs time using the Power Law model and the Carreau model in the SF and AC regions, V=50 mm/s, ε=0.5, k=0.8, β=2.6E-8.

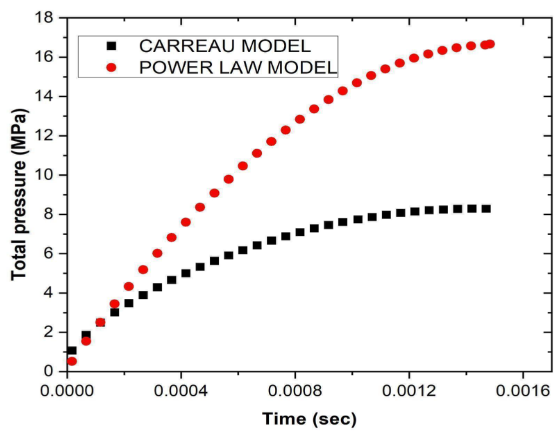

Figure 8. Total pressure vs time in the SF region using the models of Power Law and Carreau, V=50 mm/s, ε =0.5, k=0.8, β=2.6E-8.

The highest velocities are found in the SF zone for both non-Newtonian models (see Fig. 5). In this area the fluid moves without restrictions, and it develops freely and can reach velocities close to 0.1 m/s in this case. Being a non-Newtonian fluid (pseudoplastic one), the viscosity decreases with increasing shear rate, allowing higher speeds to be reached in the SF region. In the case of the AC region, only a percentage of the volume is fluid; for these results, k = 0.8, which is equivalent to 80% of the volume being occupied by fluid. Therefore, the available effective area is reduced as viscous resistance increases. It reduces the velocity of the fluid, as it must be distributed through a smaller space. In this region, velocities reached values of around 1.0E-4 m/s.

Fig. 8 shows the total pressure measured in P_{SF} as a function of time for the two non-Newtonian models. In this figure, it can be observed that the highest-pressure values were obtained using the Power Law model, where maximum pressure values of approximately 17 MPa were reached, unlike the

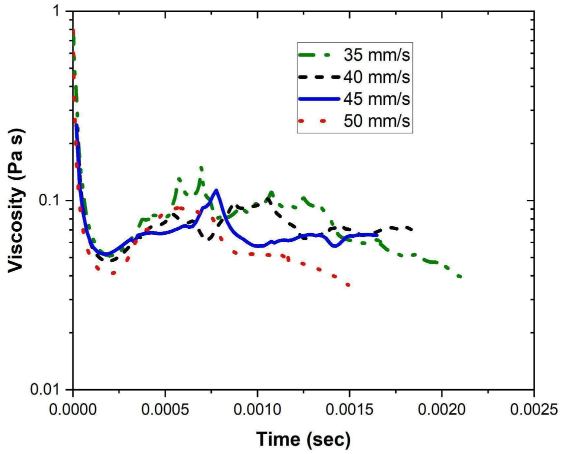

Figure 9. Viscosity vs time when varying the velocity of the moving wall in the SF region from 35 mm/s to 50 mm/s, ε=0.5, k=0.8, β=2.6E-8, for the Carreau model.

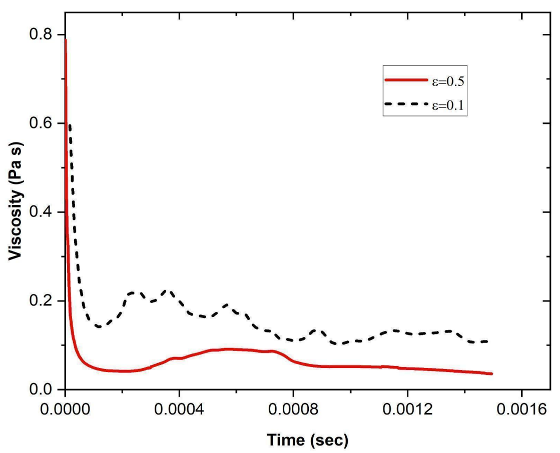

Figure 10. Viscosity vs time in the SF zone varying the dimensionless displacement (ε), V=50 mm/s, k=0.8, β=2.6E-8, for the Carreau model.

Carreau model, where maximum values of 8 MPa were obtained. This pressure variation can be assumed to be due to the functional form of the Carreau model, which involves a relaxation parameter (λ), allowing for smoother viscosity variations. Therefore, the Carreau model can capture a wider range of fluid behaviors, from low to high shear rates. This means that during shear rate transitions, the Carreau model adjusts viscosity and significantly reduces flow resistance. This ability of the Carreau model to adjust more dynamically to different flow regimes results in a lower pressure generation in the system.

The fluid dynamics using the Carreau model are analyzed, with the velocity of the moving wall (V), the dimensionless displacement (ε), the porosity (k), and the permeability (β) varied. Fig. 9 shows the viscosity results in the SF region as a function of time when varying the moving wall velocity. According to experimental data obtained by Smith (2018), the viscosity values decay rapidly, reaching a minimum of approximately 0.05 Pa · s. Afterwards, the viscosity oscillates around the minimum and remains with values below 0.1 Pa·s. It can be observed that as the speed of the moving wall increases, the total time for displacement decreases as expected.

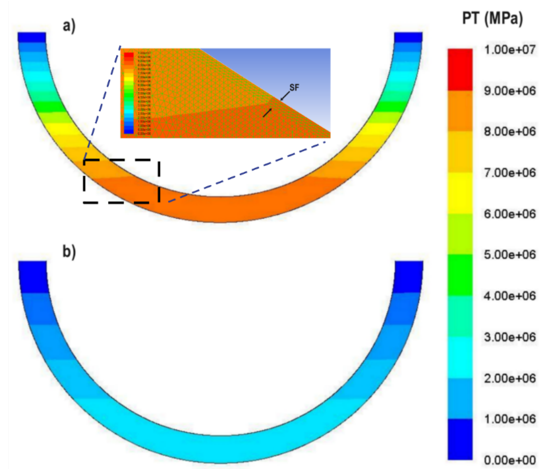

Figure 11. Total pressure distribution throughout the system (SF and AC), V=50 mm/s, k=0.8, β=2.6E-8, Carreau model, for: (a) ε = 0.5; (b) ε = 0.1.

Fig. 10 shows the behavior of apparent viscosity when making two dimensionless displacements of the moving wall (ε = 0.1 and ε = 0.5) using the Carreau model. A dimensionless displacement of ε = 0.5 means that the moving wall was displaced by 50% of the thickness of the SF region, and ε = 0.1 represents a displacement of 10%. It was observed that greater displacement of the moving wall results in a lower apparent viscosity because the fluid can reach higher velocities. At a moving wall displacement of ε = 0.5, the viscosity rapidly decreases to values of 0.05 Pa·s, which corresponds to the minimum value defined in the Carreau model. For a dimensionless displacement of ε = 0.1, the viscosity reached values around 0.1 Pa·s at the end of the displacement.

Fig. 11 shows the total pressure contours reached at the end of the moving wall displacement when ε varies. The figure on the left shows the pressure distribution reached throughout the system (SF and AC) when ε = 0.5. Therefore, the thickness of the SF region is reduced by 50%. The highest pressure is obtained in the lower part of the geometry, where the greatest deformation occurs. The maximum pressures reached are on the order of 8 MPa. On the other hand, when ε = 0.1, the maximum pressure reached is 2 MPa. Since the thickness ratio between SF and AC regions is much less than 1 (d/D « 1), on the order of 1E-2, the scales do not allow the entire pressure distribution to be visualized only in the LS region. However, the pressure values are remarkably similar to those observed in the AC region near the LS region, as evident from a zoomed-in view of a small

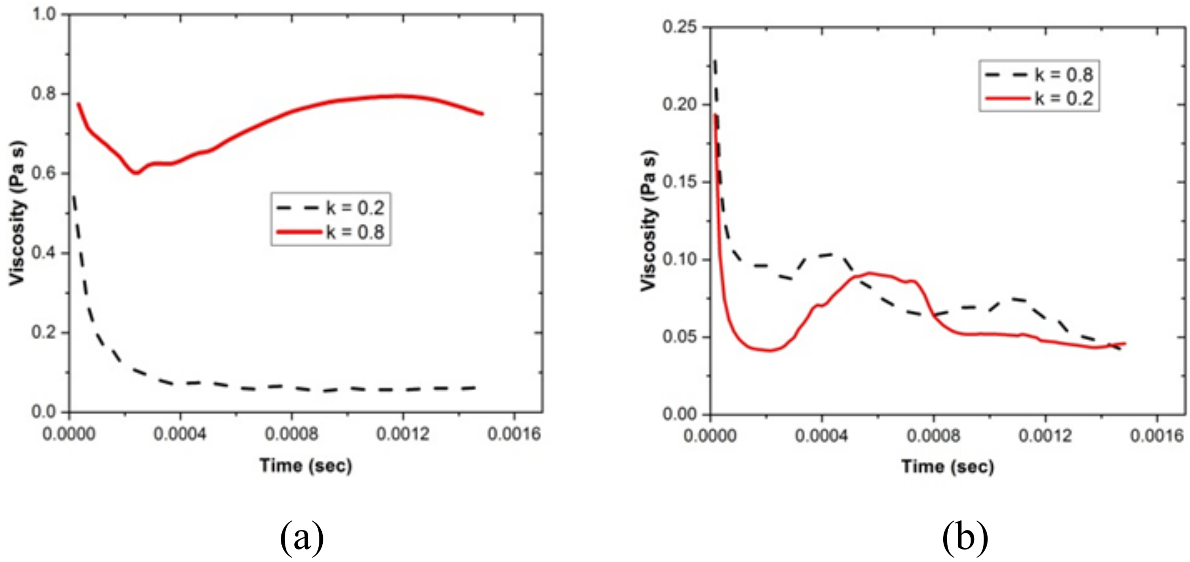

Figure 12. Viscosity vs time for different porosity values in the region of a) AC, b) SF, using the Carreau model, V=50 mm/s, ε=0.5, β=2.6E-8.

section of the interface within the synovial cavity. For displacements generated by the moving wall, the highest risk area is located along the axis of symmetry, where the maximum pressure value coincides with the greatest thinning in LS thickness. This behavior may be related to rapid or high-impact joint movements, such as those occurring during jumping actions, where the sudden increase in load and the temporary reduction in synovial fluid thickness promote stress concentration in that region (Eschweiler *et al*., 2021).

Two porosity values with k=0.2 and k=0.8 were studied in the synovial cavity. Fig. 12 shows the influence of porosity on viscosity for non-Newtonian behavior for the Carreau model. Fig. 12(a) shows the results obtained in the AC region. For the case of low porosity with k=0.2, it can be observed that viscosity drops drastically until reaching a value close to 0.1 Pa·s. While for high porosity with k=0.8, the viscosity remains in a range of 0.6 - 0.8 Pa·s. Fig. 12(b) shows the viscosity behavior in the SF zone, where for both porosity values the viscosity rapidly decays in a very short period. The lowest viscosity values are reached at a porosity of k=0.2, quickly reaching the value of 0.05 Pa·s. On the other hand, for a porosity of k=0.8, after the rapid drop in viscosity, there is a less abrupt decrease until the value of 0.05 Pa·s is reached. In media with lower porosity, fluid flow is more restricted, which increases the local shear rate. The Carreau model is more sensitive to these changes and therefore predicts a remarkable reduction in viscosity. As the model captures the transition from the apparent viscosity at the maximum viscosity value (η_0 = 0.8) to the minimum viscosity value (η_∞= 0.052), under high deformation conditions, which are more common in porous media with smaller pores, it is possible to appreciate the viscosity reduction in detail. Therefore, the effect of the change in porosity is more noticeable in the cartilage region, as can be seen in Fig. 12(a).

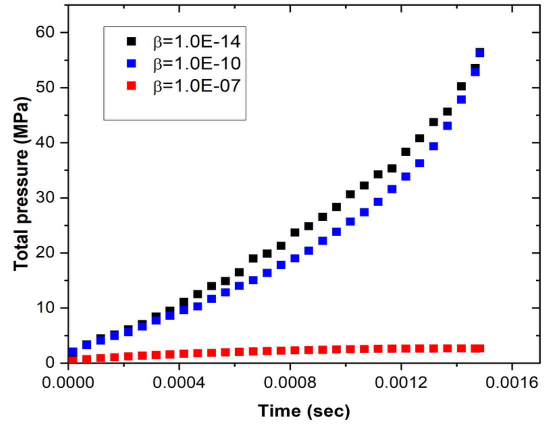

Figure 13. Total pressure vs time in the SF zone, varying the permeability, V=50 mm/s, ε=0.5, k=0.8, using the Carreau model.

Once the variation in viscosity regarding porosity in the AC zone was obtained, the influence of permeability on the system was analyzed. Permeability in the AC zone was varied with three values (β =1.0E−14, β =1.0E−10, β =1.0E−07), and the total pressure in the SF zone was monitored. Fig. 13 shows the variation in permeability and shows that decreasing permeability reduces the fluid's ability to move freely, which affects the pressure profile and the local shear rate. Therefore, pressure and permeability are related: the lower the permeability, the higher the total pressure.

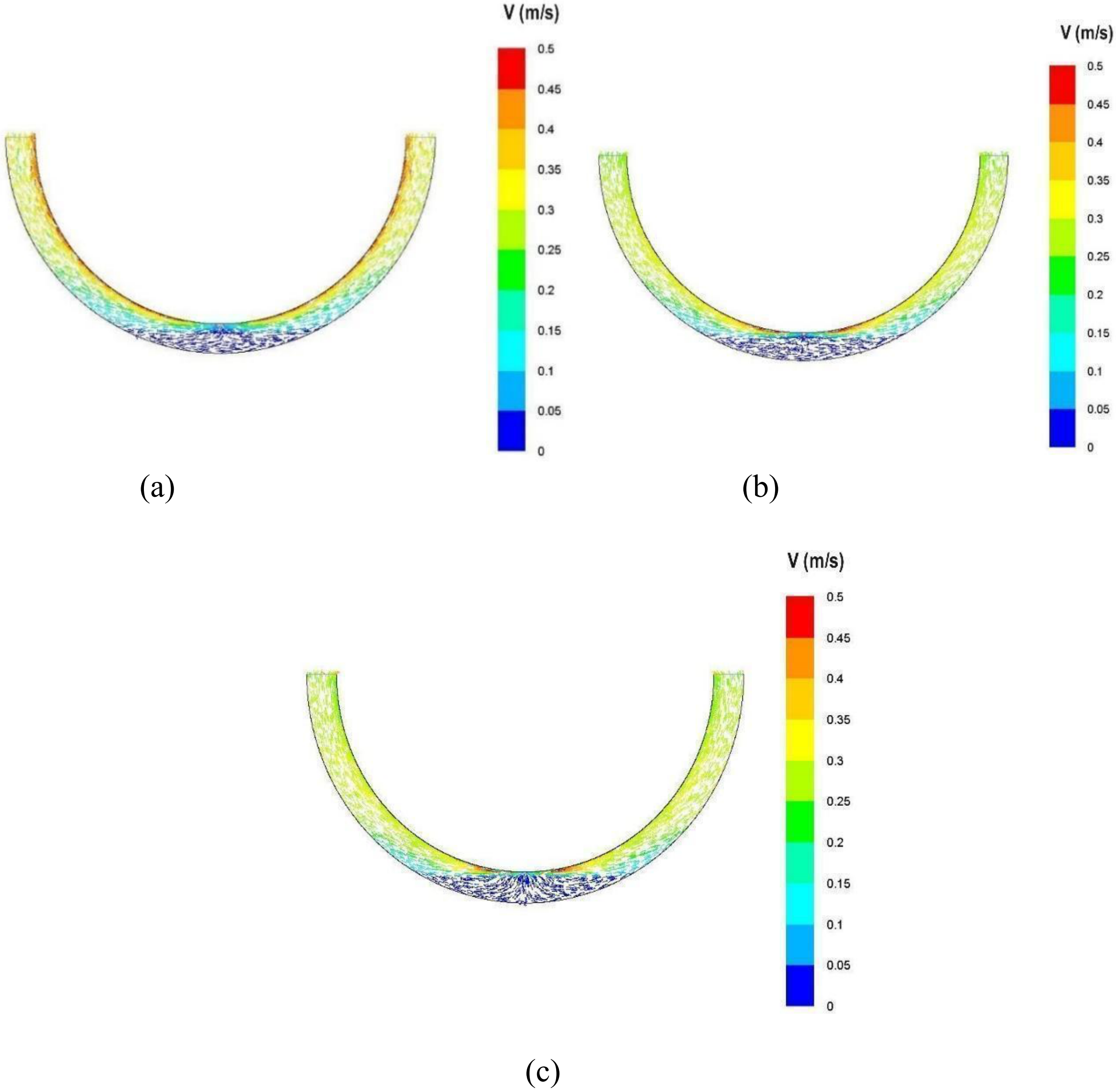

Figure 14. Distribution of velocity vectors in the whole system (SF and AC regions), V=50 mm/s, ε=0.5, k=0.8, β=2.6E-8, for: (a) Carreau model, (b) Power Law model, and (c) Newtonian model with viscosity of 0.6 Pa·s.

Fig. 14 shows the distribution of velocity vectors for the Carreau, Power Law, and Newtonian models, the latter for a viscosity of μ = 0.6 Pa·s. It is observed that the highest velocity values across the whole system are obtained with the Carreau model. On the other hand, very similar behavior was obtained in the velocity vector distribution for Power Law and Newtonian models. In all three models, the highest velocities are found in the SF region, reaching magnitudes of up to 0.5 m/s. It is also observed that there is a region of low mobility in the central part of the AC region, with velocities of the order of 0.05 m/s.

The distribution of velocity vectors shown in Fig. 14 illustrate a fluid film lubrication mechanism typical of a healthy joint, where minimum velocities are in the cartilage zone and increase in the fluid region. This behavior reflects the ability of synovial fluid to absorb mechanical loads and dissipate energy through shear stresses. (Lin & Klein, 2021; Farnham *et al.*, 2021). From a biomechanical perspective, this flow helps protect the joint, ensuring smooth movement and reducing wear (Klein, 2013).

Fig. 15 illustrates the flow of synovial fluid throughout the synovial cavity, which can be related to the cartilage nutrition process by modifying the fluid distribution in the cartilage. Tissue porosity significantly influences fluid transport capacity within the porous matrix. A low porosity (k = 0.2) limits fluid movement, restricting nutrient exchange. In contrast, a high porosity (k = 0.8) allows for greater penetration

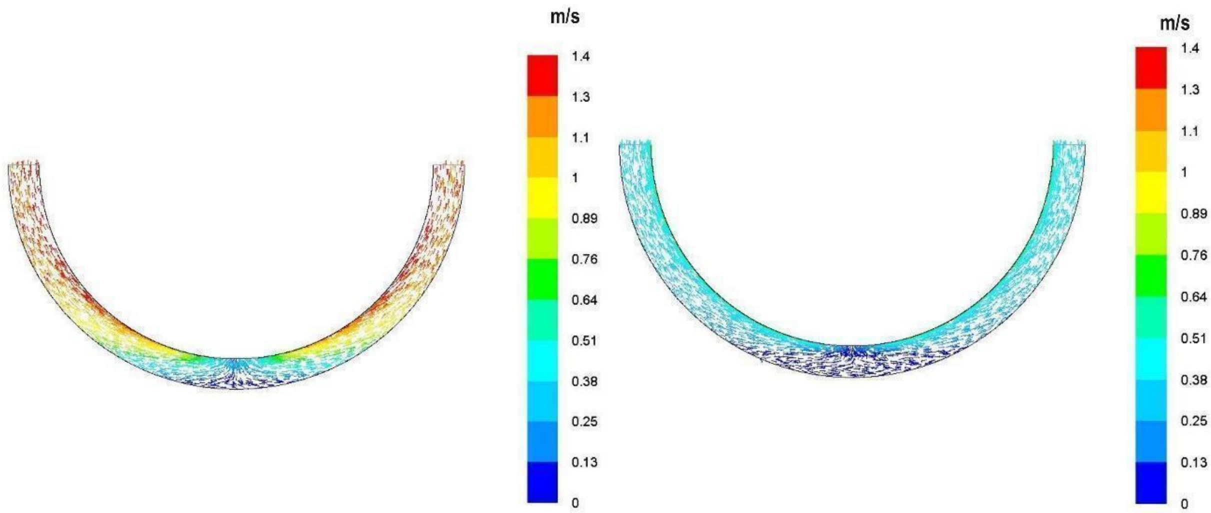

(a) (b)

Figure 15. Distribution of velocity vectors in the whole system, V=50 mm/s, ε=0.5, β=2.6E-8, using the Carreau model, for: a) k = 0.2; b) k = 0.8.

and longer contact time of synovial fluid, enhancing tissue nutrition and regeneration. These findings support the idea of "exudation lubrication," where load-driven fluid movement helps provide nutrients to cartilage (McNary *et al*., 2012). When cartilage porosity decreases, fluid transport is restricted, compromising joint lubrication and increasing friction and contact stresses. This is associated with osteoarthritis, a degenerative disease in which cartilage degradation and rheological changes in the synovial fluid lead to poor lubrication and increased joint degeneration (Rajankunte Mahadeshwara *et al*., 2024).

4 Discussion

The results obtained from numerical modeling of synovial fluid, using Newtonian and non-Newtonian models, provide a better understanding of how fluid rheology affects intra-articular dynamics, especially under deformation conditions. The observed decrease in viscosity for non-Newtonian models, particularly at high shear rates, is consistent with the pseudoplastic nature of synovial fluid reported in the literature (Rebenda *et al*., 2020; (Rinaudo *et al*., 2009) *et al*., 2009; Roškar *et al*., 2025; Simou *et al*., 2022) This effect is more remarkable in the Power Law Model, due to its mathematical simplicity and the absence of transition terms; in contrast, the Carreau model offers a more gradual and physiologically realistic response, due to the implementation of the relaxation parameter.

A notable observation is the behavior of synovial fluid at different porosity values in the cartilage region. A porosity of k=0.2 leads to a significant increase in fluid velocity, both in the synovial fluid (SF) and articular cartilage (AC) regions. This, in turn, contributes to a rapid decrease in apparent viscosity, especially with the Carreau model (Bowers & Miller, 2023). This phenomenon can be explained by the concentration of flow lines in a small space. This increases the local shear rate and intensifies the fluid's non-Newtonian behavior. These results are consistent with the expectations derived from the literature. (de Boer *et al*., 2020; Jithin *et al*., 2018; Martin-Alarcon *et al*., 2024).

The highest pressures were recorded in systems with higher viscosity or lower permeability, suggesting greater resistance to flow and, therefore, a possible increase in joint loading during movement. These results could be related to pathologies such as osteoarthritis, where cartilage permeability may be reduced due to degenerative processes. However, this topic will be discussed in future work.

Another significant result is the impact of the moving wall's displacement velocity and deformation distance on the fluid's rheological behavior. At higher velocities and deformations, a more pronounced decrease in viscosity and an increase in total pressure were observed. These results highlight the sensitivity of synovial fluid behavior to dynamic mechanical loads, reinforcing the importance of modeling these systems under transient conditions rather than steady-state conditions.

It could be observed that although the Power

Law model exhibited abrupt changes in viscosity and pressure, the Carreau model exhibited more moderate behavior, making it more suitable for simulating synovial fluid. The distribution of velocity vectors confirms the advantage of the Carreau model in allowing higher peak velocities without compromising flow continuity, thereby improving predictions of articular cartilage lubrication.

Compared to a 3D model, the two-dimensional model provides an initial approximation that enables analysis of the hydrodynamic and rheological behavior of synovial fluid and articular cartilage with minimal computational effort. It captures general trends, such as the relationships among porosity, permeability, and velocity, as well as the fluid pseudoplastic behavior, thereby approximating real-life behavior. In the 3D model, due to its more complex curved geometry and stress distribution (which includes spatial gradients, anisotropic deformations, and localized shear rate zones affecting lubrication mechanisms), the computational times will be significantly longer. Therefore, the 2D approach is valuable for preliminary studies and numerical validations. Furthermore, it establishes a computational foundation for transferring the principles of biological lubrication to engineering design. The numerical results derived from the analysis of synovial fluid can guide the development of high performance lubricants, prosthetic materials, and mechanical systems that operate under extreme conditions, promoting greater efficiency and durability through optimized designs. Taken together, these findings underscore the importance of integrating physical modeling and computational simulation to understand biological lubrication processes. By linking rheology, biomechanics, and engineering design, this study contributes to a broader understanding of how nature-inspired principles can lead to more efficient and sustainable technological solutions.

In a three-dimensional configuration, curved joint surfaces generate spatial pressure gradients and localized regions with high shear rates that cannot be captured in a two-dimensional model. Furthermore, the inherent asymmetry in a real geometry of joints (Freeman & Pinskerova, 2003) accentuates these effects, resulting in more complex and non-homogeneous pressure distributions. Consequently, although the 2D model used in this study qualitatively agrees with the central pressure trend, it may underestimate the maximum stresses and the pressure and velocity distributions observed in realistic geometries. The two-dimensional formulation employed in this study should be interpreted as a computational approximation that preserves the essential hydrodynamic behavior, subject to the limitations noted above.

Conclusions

In this work, the fluid region of a synovial cavity, composed of a thin layer of synovial fluid (SF) attached to articular cartilage (AC), was modeled. Different Newtonian and non-Newtonian models for representing synovial fluid were compared.

The non-Newtonian Carreau model, with a relaxation parameter (λ), yielded smoother viscosity transitions during deformation. The Carreau model produced higher fluid velocities in SF and AC compared to the Power Law or Newtonian models. However, both non-Newtonian models showed similar viscosity behavior over time when porosity is varied. The maximum pressure value increased as permeability decreased in AC. A larger dimensionless displacement (ε) caused significant viscosity decreases when higher fluid velocities occurred during moving wall displacement. This displacement thinned the central SF area, increasing total pressure. Over a range of moving wall velocities (35 to 50 mm/s), viscosity decreased dramatically from 0.8 to 0.05 Pa·s for all cases.

The power-law model is widely used to simulate biological fluids, such as synovial fluid, due to its simple mathematical expression. However, it lacks temperature-dependent terms, limiting its realistic representation of rheological behavior. The Carreau model, an extension of the power law, provides a more complete description of shear values and better fits experimental data. Further work will compare the two non-Newtonian models studied here in greater detail. Another issue to consider as future investigations will take into account the distribution of velocity vectors and pressure concentrators in a more realistic geometry that will involve aspects of dissymmetry, such as the difference in the radii of the condyles or wear in the thicknesses of the cartilage derived from some disease.

This work contributes to a better understanding of synovial fluid behavior. Modeling SF as a non-Newtonian fluid in porous media using numerical tools enables the simulation of biological systems and a wide range of industrial processes involving rheological studies.

Acknowledgements

The authors want to thank Secretary of Government SECIHTI (before CONACyT) one scholarship received for the postgraduate student and the support received from the Coordination of Scientific Research of Universidad Michoacana de San Nicolás de Hidalgo (CIC-UMSNH).

References

Abraham, A. M., & Venkatesan, S. (2023). A review on application of biomaterials for medical and dental implants. Proceedings of the Institution of Mechanical Engineers, Part L: Journal of Materials: Design and Applications, 237(2), 249-273. https://10.1177/14644207221121981

Bear Jacob. (1972). *Dynamics of Fluids in Porous Media* (first edition).

Botu, V., Batra, R., Chapman, J., & Ramprasad, R. (2017). Machine learning force fields: construction, validation, and outlook. The Journal of Physical Chemistry C, 121(1), 511-522. https://doi.org/10.1021/acs.jpcc.6b10908

Bowers, C. A., & Miller, C. T. (2023). Modeling flow of Carreau fluids in porous media. *Physical Review E*, *108*(6). https://doi.org/10.1103/PhysRevE.108.065106

Brannan, S. R., & Jerrard, D. A. (2006). Synovial fluid analysis. *The Journal of emergency medicine*, *30*(3), 331-339. https://doi.org/10.1016/j.jemermed.2005.05.029

Brujan, E. A. (2011). Non-Newtonian Fluids. In *Cavitation in Non-Newtonian Fluids: With Biomedical and Bioengineering Applications*, 1-47. Springer, Berlin, Heidelberg. https://doi.org/10.1007/978-3-642-15343-3_1

Chhimwal, J., Jangid, P., Kumar, D., Kumar, V., & Kumar, R. (2023). To study and develop the mathematical models to review the properties of synovial fluids. *Materials Today: Proceedings*. https://doi.org/10.1016/j.matpr.2023.01.246

de Boer, G. N., Raske, N., Soltanahmadi, S., Dowson, D., Bryant, M. G., & Hewson, R. W. (2020). A porohyperelastic lubrication model for articular cartilage in the natural synovial joint. *Tribology International*, *149*. https://doi.org/10.1016/j.triboint.2019.04.044

Eschweiler, J., Horn, N., Rath, B., Betsch, M., Baroncini, A., Tingart, M., & Migliorini, F. (2021). The biomechanics of cartilage—An overview. *Life*, *11*(4), 302. https://doi.org/10.3390/life11040302

Farnham, M. S., Ortved, K. F., Horner, J. S., Wagner, N. J., Burris, D. L., & Price, C. (2021). Lubricant Effects on Articular Cartilage Sliding Biomechanics Under Physiological Fluid Load Support. *Tribology Letters*, *69*(2). https://doi.org/10.1007/s11249-021-01430-0

Fuentes-Cortés, L. F., Flores-Tlacuahuac, A., & Nigam, K. D. (2022). Machine learning algorithms used in PSE environments: A didactic approach and critical perspective. *Industrial & Engineering Chemistry Research*, *61*(25), 8932-8962. https://doi.org/10.1021/acs.iecr.2c00335.

Freeman, M. A. R., & Pinskerova, V. (2003). The movement of the knee studied by magnetic resonance imaging. *Clinical Orthopaedics and Related Research*, *410*, 35–43. https://doi.org/10.1097/01.blo.0000063598.67412.0d

Giurazza, G., Caria, C., Campi, S., Franceschetti, E., Papalia, G. F., Basciani, S., Zampoli. A., Gregori, P., Papalia, R., & Marinozzi, A. (2024). Femoral cartilage thickness measured on MRI varies among individuals: Time to deepen one of the principles of kinematic alignment in total knee arthroplasty. A systematic review. *Knee Surgery, Sports Traumatology, Arthroscopy*. https://doi.org/10.1002/ksa.12408

Halonen, K. S., Mononen, M. E., Jurvelin, J. S., Töyräs, J., Salo, J., & Korhonen, R. K. (2014). Deformation of articular cartilage during static loading of a knee joint–experimental and finite element analysis. *Journal of biomechanics*, *47*(10), 2467-2474. https://doi.org/10.1016/j.jbiomech.2014.04.013

Hasnain, S., Abbas, I., Al-Atawi, N. O., Saqib, M., Afzaal, M. F., & Mashat, D. S. (2023). Knee synovial fluid flow and heat transfer, a power law model. Scientific Reports, 13(1), 18184. https://doi.org/10.1038/s41598-023-44482-z

Holmberg, K., & Erdemir, A. (2017). Influence of tribology on global energy consumption, costs and emissions. In *Friction* (Vol. 5, Issue 3, pp. 263–284). Tsinghua University Press. https://doi.org/10.1007/s40544-017-0183-5

Ingham Derek B, B. A. M. E. P. L. (Ed.). (2003). *Emerging Technologies and Techniques in Porous Media*. Science Series II, Mathematics,Physics and Chemistry.

Jithin, M.,Kumar,N.,De, A., and Das, M.K. (2018). Pore-Scale Simulation of Shear Thinning Fluid Flow Using Lattice Boltzmann Method. Transport in Porous Media, 121(3), 753-782.

https://doi.org/10.1007/s11242-017-0984-z

Jurczak, P. (2006). Pressure distribution in a squeeze film biobearing lubricated by a synovial fluid. *Applied Mechanics and Engineering*, *11*(4), 857.

Kraus, V. B., Stabler, T. V., Kong, S. Y., Varju, G., & McDaniel, G. (2007). Measurement of synovial fluid volume using urea. *Osteoarthritis and cartilage*, *15*(10), 1217-1220. https://doi.org/10.1016/j.joca.2007.03.017

Křen, J., & Hynčík, L. (2007). Modelling of non-Newtonian fluids. *Mathematics and Computers in Simulation*, *76*(1-3), 116-123. https://doi.org/10.1016/j.matcom.2007.01.006

Kumavat, R., Kumar, V., Malhotra, R., Pandit, H., Jones, E., Ponchel, F., & Biswas, S. (2021). Biomarkers of joint damage in osteoarthritis: current status and future directions. *Mediators of Inflammation*, *2021*(1), 5574582. https://doi.org/10.1155/2021/5574582

Liao, J., Miramini, S., Liu, X., & Zhang, L. (2020). Computational study on synovial fluid flow behaviour in cartilage contact gap under osteoarthritic condition. *Computers in Biology and Medicine*, *123*, 103915. https://doi.org/10.1016/j.compbiomed.2020.103915

Lin, W., & Klein, J. (2021). Recent Progress in Cartilage Lubrication. In *Advanced Materials* (Vol. 33, Number 18). John Wiley and Sons Inc. https://doi.org/10.1002/adma.202005513

Madkhali, A., Chernos, M., Grecov, D., & Kwok, E. (2016). Osteoarthritic synovial fluid rheology and correlations with protein concentration. *Biorheology*, *53*(3-4), 111-122. https://doi.org/10.3233/BIR-15078

Märtens, N., März, V., Bertrand, J., Lohmann, C. H., & Berth, A. (2022). Radiological changes in shoulder osteoarthritis and pain sensation correlate with patients' age. *Journal of Orthopaedic Surgery and Research*, *17*(1), 277. https://doi.org/10.1186/s13018-022-03137-x

Martin-Alarcon, L., Govedarica, A., Ewoldt, R. H., Bryant, S. L., Jay, G. D., Schmidt, T. A., & Trifkovic, M. (2024). Scale-Dependent Rheology of Synovial Fluid Lubricating Macromolecules. *Small*, *20*(21). https://doi.org/10.1002/smll.202306207

Martínez-Gutiérrez, N., Ibarra-Bracamontes, L. A., Galván-González, S. R., Aguilar-Corona, A., & Viramontes-Gamboa, G. (2016). Numerical Modeling of the Knee Synovial Joint Under Deformation Using the Finite Volume Method. In *Recent Advances in Fluid Dynamics with Environmental Applications* (pp. 419-433). Springer International Publishing. https://doi.org/10.1007/978-3-319-27965-7_30

Mathieu, P.,Conrozier T.,E.,Rozand, Y., and Rinaudo, M (2009). Rheologic Behavior of Osteoarthritis Synovial Fluid after Addition of Hyaluronic Acid: A Pilot Study. Clinical Orthopaedics and Related Research, 467 (11), 3002-3009. https://doi.org/10.1007/s11999-009-0867-x

Moghadam, M. N., Abdel-Sayed, P., Camine, V. M., & Pioletti, D. P. (2015). Impact of synovial fluid flow on temperature regulation in knee cartilage. *Journal of biomechanics*, *48*(2), 370-374. https://doi.org/10.1016/j.jbiomech.2014.11.008

Nield, D. A., & Bejan, A. (2013). Mechanics of Fluid Flow Through a Porous Medium. In *Convection in Porous Media* (pp. 1–29). Springer New York. https://doi.org/10.1007/978-1-4614-5541-7_1

Norton, R. L. (2009). *Kinematics and Dynamics of Machinery* (McGraw-Hill.).

Oei, E. H. G., Hirvasniemi, J., van Zadelhoff, T. A., & van der Heijden, R. A. (2022). Osteoarthritis year in review 2021: imaging. *Osteoarthritis and Cartilage*, *30*(2), 226-236. https://doi.org/10.1016/j.joca.2021.11.012

Oliviero, F., and Mandell, B. F. (2023). Synovial fluid analysis: Relevance for daily clinical practice. Best Practice & Research Clinical Rheumatology, 101848. https://doi.org/10.1016/j.berh.2023.101848

Ouerfelli, N., Vrinceanu, N., Mliki, E., Amin, K. A., Snoussi, L., Coman, D., & Mrabet, D. (2024). Rheological behavior of the synovial fluid: a mathematical challenge. *Frontiers in Materials*, *11*, 1386694. https://doi.org/10.3389/fmats.2024.1386694

Pearce, D., Fischer, S., Huda, F., & Vahdati, A. (2020). Applications of computer modeling and simulation in cartilage tissue engineering. *Tissue engineering and regenerative medicine*, *17*, 1-13. https://doi.org/10.1007/s13770-019-00216-9

Perruccio, A. V., Young, J. J., Wilfong, J. M., Power, J. D., Canizares, M., & Badley, E.

M. (2024). Osteoarthritis year in review 2023: Epidemiology & therapy. Osteoarthritis and Cartilage, 32(2), 159-165. https://doi.org/10.1016/j.joca.2023.11.012

Pekkan, K., Nalim, R., & Yokota, H. (2003, January). Computed synovial fluid flow in a simple knee joint model. In *Fluids Engineering Division Summer Meeting* (Vol. 36967, pp. 2085-2091). https://doi.org/10.1115/FEDSM2003-45430

Rajankunte Mahadeshwara, M., Al-Jawad, M., Hall, R. M., Pandit, H., El-Gendy, R., & Bryant, M. (2024). How Do Cartilage Lubrication Mechanisms Fail in Osteoarthritis? A Comprehensive Review. *Bioengineering*, *11*(6), 541. https://doi.org/10.3390/bioengineering11060541

Rebenda, D., Vrbka, M., Ćípek, P., Toropitsyn, E., Nećas, D., Pravda, M., & Hartl, M. (2020). On the dependence of rheology of hyaluronic acid solutions and frictional behavior of articular cartilage. *Materials*, *13*(11). https://doi.org/10.3390/ma13112659

Rinaudo, M., Rozand, Y., Mathieu, P., & Conrozier, T. (2009). Role of Different Pre-Treatments on Composition and Rheology of Synovial Fluids. *Polymers*, *1*(1), 16–34. https://doi.org/10.3390/polym1010016

Roškar, S., Mihalič, R., Mihelič, A., & Trebše, R. (2025). Synovial fluid viscosity with synovial fluid cell count, valuable diagnostic marker of prosthetic joint infections. *Scientific Reports*, *15*(1). https://doi.org/10.1038/s41598-025-00760-6

Sadique, M., & Shah, S. R. (2022). Mathematical study for the synovial fluid flow in Osteoarthritic knee joint. *Journal of Engineering and Applied Sciences*, *17*(2), 15-21.

Sajan, A., Mehta, T., Griepp, D. W., Chait, A. R., Isaacson, A., & Bagla, S. (2022). Comparison of minimally invasive procedures to treat knee pain secondary to osteoarthritis: a systematic review and meta-analysis. *Journal of Vascular and Interventional Radiology*, *33*(3), 238-248. https://doi.org/10.1016/j.jvir.2021.11.004

Siddiqui, A. M., Maqbool, K., Ahmed, A., & Mann, A. B. (2025). Inertial and Linear Re-Absorption Effects on a Synovial Fluid Flow Through a Lubricated Knee Joint. *Lubricants*, *13*(5). https://doi.org/10.3390/lubricants13050196

Simou, K., Jones, S. W., Davis, E. T., Preece, J., & Zhang, Z. J. (2022). Rheological and interface adhesive properties of osteoarthritic synovial fluids. *Biotribology*, *32*. https://doi.org/10.1016/j.biotri.2022.100227

Smith, A. M., Fleming, L., Wudebwe, U., Bowen, J., & Grover, L. M. (2014). Development of a synovial fluid analogue with bio-relevant rheology for wear testing of orthopaedic implants. *Journal of the mechanical behavior of biomedical materials*, *32*, 177-184. https://doi.org/10.1016/j.jmbbm.2013.12.009

Yeoh, G.H & Yuen, K.K (2009). Computational Fluid dynamics in fire engineering: modelling and practice.

Walicki, E., & Walicka, A. (2000). Mathematical modelling of some biological bearings. *Smart Materials and Structures*, *9*(3), 280–283. https://doi.org/10.1088/0964-1726/9/3/305

Walicki, E., & Walicka, A. (2002). Inertia and couple-stress effects on squeeze-film characteristics with reference to biological bearings. *TriboTest*, *8*(3), 195-203. https://doi.org/10.1002/tt.3020080302

Walicka, A., & Walicki, E. (2004). Pressure distribution in a curvilinear hydrostatic bearing lubricated by a micropolar fluid in the presence of a cross magnetic field. *Lubrication Science*, *17*(1), 45–52. https://doi.org/10.1002/ls.3010170104

Zambrano-Rangel, R., Rico-Ramirez, V., & Iglesias-Silva, G. A. (2019). Experimental measurement of blood physical properties and its application to blood flow simulation. *Revista Mexicana de Ingeniería Química*, *18*(2), 621-636.

Ziylan, T., & Murshed, K. A. (2002). An analysis of Anatolian human femur anthropometry. *Turkish Journal of Medical Sciences*, *32*(3), 231-235.